

Observations of Ice-Crushing Phenomena under a Skate Blade

Robert Gagnon
OCRE/NRC, St. John's, Canada

ABSTRACT

Experiments using a mock ice-skating blade have shown that when the blade is sliding laterally on an ice surface at 30 mm/s, similar to a skater applying a pushing stride to accelerate or when stopping, crushing produces regular spallation events at the intact-ice/blade interface (where pressure is ~ 50 MPa) that result in a cyclic load pattern (spalling frequency ~ 85 Hz). During forward gliding there was also evidence of spallation events at the gently-upturned 'bow' of the blade (spalling frequency ~ 39 Hz). From the speed and force data, and the depths of the lateral shaving and the forward gliding track profile, the energy consumed per unit volume of ice removed was determined in both cases. The energy budget implied that 12% of the shaved ice material was liquid melt, and 18% of the thin sheet-like slurry of liquid and ice particles (< 0.1 mm thickness) extruding from the edges of the blade-bow during gliding was melt. More energy per unit volume was consumed in the gliding case because all spallation debris at the bow was removed from the track by high-pressure compaction imposed by the over-running blade. This caused further pulverization and inter-particle ice-on-ice crushing generating mobile slurry that augmented slurry produced on intact-ice hard-zone areas at the blade-ice interface. In the lateral shaving case less material was converted to slurry because many unconfined pieces of the shattered spalls were not subjected to further pulverization/extrusion. This was evident from the post-test observation of the accumulated shaved material that showed spall debris mixed with refrozen extruded slurry. The crushing of ice and presence of slurry under a skate blade are important observations because earlier ice crushing-friction experiments have shown that a thin (< 0.2 mm) highly-lubricating slurry (~ 16 % liquid) is produced at high-pressure hard-zone contact regions, which facilitates extremely low friction.

KEY WORDS: Ice crushing; Skate blade; Ice-liquid slurry.

INTRODUCTION

Ice skating is a fascinating subject. Previous studies have described some of the physics analytically with varying degrees of success (e.g. Le Berre and Pomeau, 2015; Lozowski et al., 2013; Van Leeuwen, 2017). The theories depend on the generation and action of a thin lubricating melt layer between the blade and the ice that generates heat from shear friction, and also on an element of 'ploughing' of the ice to account for rapid removal at the 'bow' of the blade. The 'ploughing' terminology is used loosely, with few physical details, since inherently-complex ice crushing of some sort is involved. However, the most current understandings of physical mechanisms involved in ice crushing, over a wide range of scales, in the brittle regime can account for rapid removal of ice from the bow of a gliding skate

blade or from the edge of a laterally sliding/shaving blade. We have conducted recent experiments using mock ice-skating blades that traversed the surface of lab-grown ice samples in the gliding and lateral-shaving orientations to look in detail at various aspects.

APPARATUS DESCRIPTION AND TEST STRATEGY

Mock skate blades, manufactured from stainless steel, were used for the tests. These had similar dimensions and characteristics in the lateral section as typical recreational blades, however, they were shorter in length (~ 40 mm) in order to optimize the lengths of the ice sample surfaces that were used. The ‘hollow’ on the bottom of the blades had a radius of curvature of 7 mm. Along its length the blade edges were linear in the central 20 mm of length and curved upwards at the 10 mm length segment at each end, with a curvature radius of 50 mm. Figure 1 shows a blade sliding from left to right on the flat surface of a columnar-grained freshwater ice sample. The track left on the ice surface following a glide test is shown in Figure 2. The reader can expand this image on-screen to see details discussed below.

Two types of tests were conducted. Gliding tests were performed by using the apparatus in load-control mode to initially press the skate onto the ice in the vertical direction. A series of normal load values (100 – 700 N, in 100 N increments) were used. The load range covers typical forces of actual skating, when taking into account that we use only a portion of the length of real skate blades. Shortly after each normal load was established the blade was slid forward in the glide direction at constant speed (30 mm/s) for a distance of about 7 cm. Ice



Figure 1. Mock ice-skating blade gliding from left to right on a columnar-grained freshwater ice sample.



Figure 2. Blade track left following a number of gliding tests. Note that the vertical load is borne on the symmetric contacting portions of the blade’s edges. The thin white wispy material is frozen extruded slurry (discussed below).

shaving experiments were also performed, where the blade was put on edge and oriented

at 45° or 90° to the sliding direction. A shaving test was conducted by first using the apparatus displacement control to initially press the skate blade edge into the ice to a certain depth that generated a load that fell into the range of loads used for the gliding tests. Shaving is what happens when a skater is accelerating during push-offs, coming to fast stops or making sharp turns. As mentioned above, we note that the blades used for the shaving tests were held in the apparatus so that one edge of the blade made contact with the ice surface, i.e. the side walls of the blade was at an angle of ~ 21° with the vertical axis. Normal load, horizontal load and displacement (vertical and horizontal) were recorded for all tests described above.

DATA ANALYSIS AND PRESENTATION

During the shaving tests it was observed that the lateral sliding/shaving of the blade led to regular intermittent movement of the blade with respect to the ice surface. The pattern of regular intermittency was also reflected in the normal load records (Figure 3). This was caused by small-scale spalling events from the ice surface (occurring at roughly 85 spalls/s, where the average spacing was ~ 0.35 mm). The regular spacing of the load peaks corresponds to the spacing of the visible remnants of the spalling events left on the ice surface (Figure 4). Ultimately the spacing of the spalls is related to the elasticity of the horizontal and vertical loading systems, and the elasticity of the ice itself. These characteristics have been shown before in lab and field-scale ice crushing and indentation experiments (e.g. Gagnon, 1999).

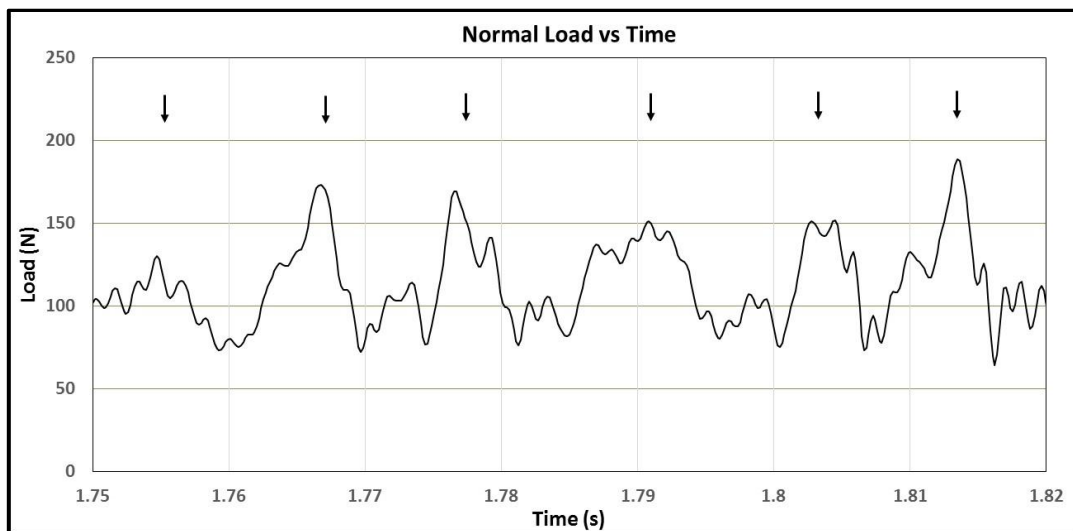


Figure 3. Normal load record associated with a test similar to that shown in Figure 4. The spacing of the six main peaks (indicated by markers) corresponds to the time spacing of the spalling events, occurring at about 85 Hz. The other lower amplitude oscillations are due to the resonant frequency of the vertical measurement/load equipment (~ 750 Hz).

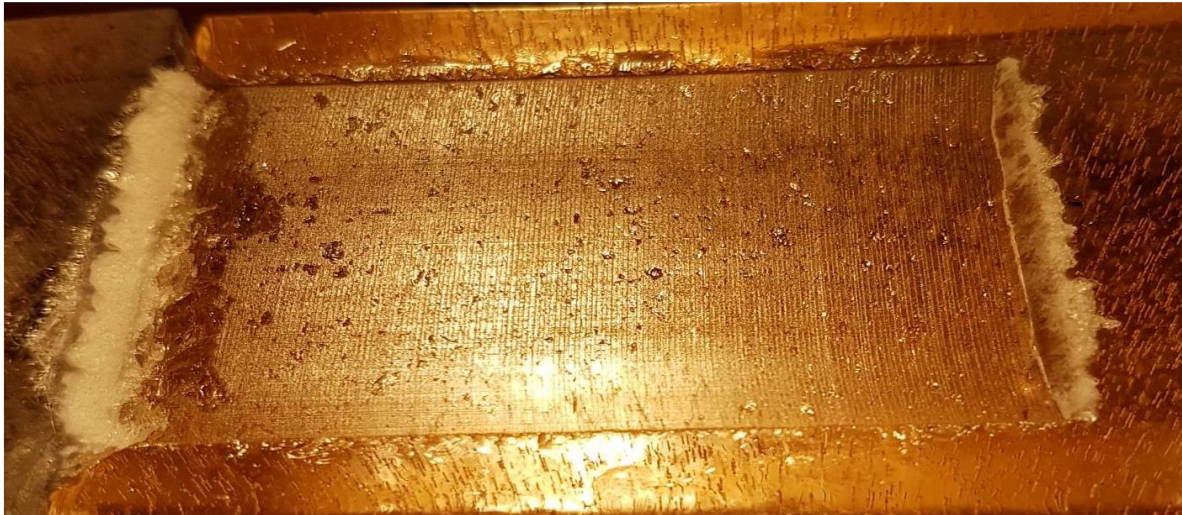


Figure 4. Ice surface following a lateral shaving test where the blade was oriented at 90° to the shaving direction. The fine tightly-spaced vertical lines correspond to a sequence of spallation events.

We have determined some characteristics of the crushed-ice material that is shaved off the ice surface. Since the depth of penetration is known for any given shaving test we can calculate the volume of ice removed from the surface during the test. Since we also know the horizontal force and the sliding/shaving displacement of the blade we can determine the energy consumed in the process. Table 1 shows the results of calculations for tests with differing blade penetrations and shaving orientations. The energy calculations imply that approximately 12% (by weight) of the ice that is shaved off is liquid melt. This should not be surprising since it has been shown in prior lab ice-crushing experiments that a thin liquid/ice-particle slurry (~ 16 % liquid [Gagnon, 2016]) is produced at the hard-zone / platen interface during crushing in the brittle regime. A similar slurry is present at inter-particle contacts as ice-on-ice crushing occurs in the matrix of crushed material that surrounds, and flows/extrudes away from, high interface-pressure hard zones during crushing.

The gliding tests that were performed with the blade may seem to be quite different from the

Table 1. Slurry-layer melt-fraction calculations.

Ice Penetration (m)	Blade Orientation To Movement Direction (degree)	Blade Travel (m)	Shaving Force (N)	Removed Ice Volume (cubic m) $\times 10^{-7}$	Dissipated Energy (J)	Heat of Fusion (J/metric ton) $\times 10^6$	Shaved Ice Melted (metric ton) $\times 10^{-7}$	Melted Ice Volume (cubic m) $\times 10^{-7}$	Removed Ice Melt Fraction (%)
0.0001	90	1	115.2	40	115.19	334	3.45	3.79	9.47
0.0001	45	1	88.3	28	88.33	334	2.64	2.91	10.27
0.00005	90	1	90.0	20	90.04	334	2.70	2.96	14.81
0.00005	45	1	63.6	14	63.63	334	1.91	2.09	14.80
							Average Melt Fraction = 12.3%		

shaving tests. However, as we shall see below, the energetics and local characteristics of ice removal at the ‘bow’ of the blade during gliding have similarities with ice shaving.

The shaving load for one typical test where the initial vertical ice penetration was 0.1 mm amounted to ~ 120 N. The ice/blade contact area (projected on the vertical plane) was 0.1 mm x 40 mm = 4 mm². Since the contacting blade surface was at about 59° from horizontal, the normal load and average pressure (from soft-zone and hard-zone ice) on the blade were ~ 140 N and ~ 35 MPa respectively. Space does not permit a full discussion of the following points, however further elaboration can be found in Gagnon (1999). Due to the transformation of high-interface pressure intact ice to low-interface pressure shattered-spall debris during repetitive spallation events, we use Figure 5 to show how the spallations lead to a reduction of intact-ice hard-zone contact area (and load) by roughly 50 %, and consequent transfer of load to the remaining intact ice due to the release of elastic stress in the ice/blade system. Hence, we would expect oscillations in the shaving load record on a similar scale, as reflected in the normal load in Figure 4. Additionally, pressure spikes (e.g. ~ 50 MPa) on the hard zone, that are significantly higher than the average pressure value on the whole contact area, at the initiation of spallation would also be expected (Gagnon, 1999; Gagnon and Tulk, 2019).

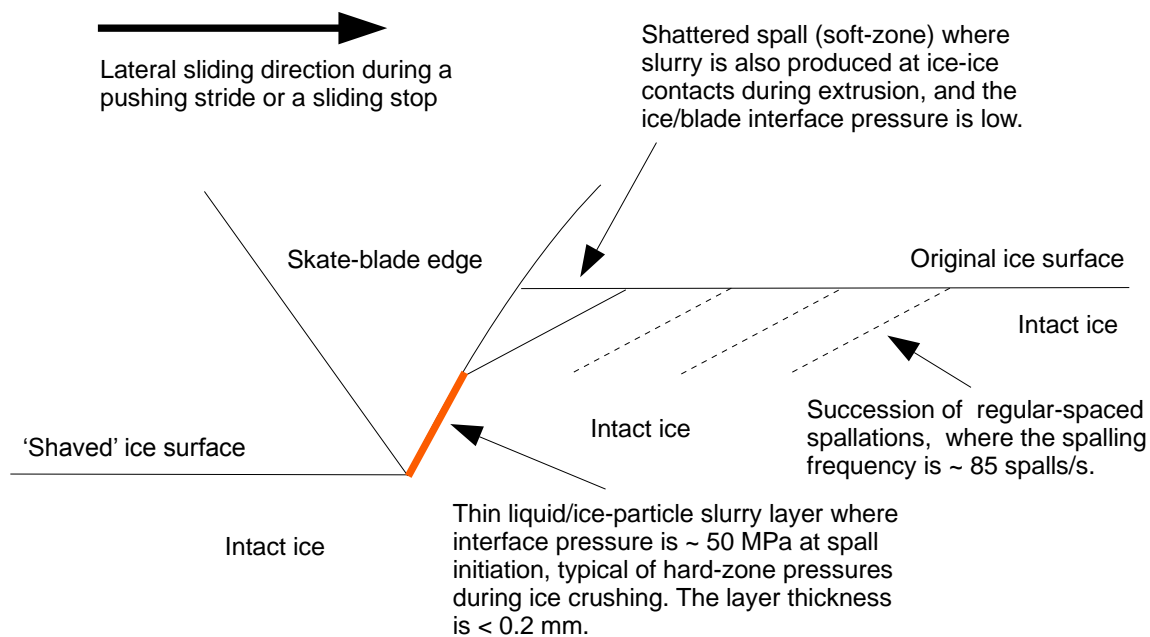


Figure 5. Skate blade on edge during a lateral sliding movement. A certain thickness of ice is removed/shaved from the original ice surface. The shaving, though on a small scale, involves common aspects of ice-crushing in the brittle regime at larger scales. These features include repetitive spallation, and a high-pressure zone of intact ice where a thin squeeze-film liquid/ice-particle slurry layer is generated. A similar process happens at the forward ‘bow’ of the skate blade during glide tests. Note that for illustrative purposes the spallation spacing is contracted and the scale of blade-depth penetration is exaggerated relative to the slurry-layer thickness.

The gliding tests were conducted as follows. A normal load (e.g. 100 N) was first applied to the blade that caused it to sink, by plasticity, to a certain depth (~ 0.051 mm) into the ice surface at the original ‘start’ location between the time when the load was applied and the glide test actually started, that is, a typical wait time of roughly 72 s. During gliding a certain amount of the work done by the system is the crushing and clearing of ice (i.e. ploughing) at the leading upturned front of the blade (the ‘bow’) to the depth that the blade had initially sunk into the ice at the start position. This clearing process provided

a track that the main body of the blade slid along behind the bow. Then the blade was slid back to the start position and a second run was conducted while the same normal load was maintained and the wait time prior to the test, since the first test, was typically ~ 30 s. Then the normal load was increased by a 100 N increment and another pair of tests were conducted in a similar manner as before. Note that during a gliding test there is negligible plastic deformation of the ice surface under the main body of the moving blade since at any particular location along the track the short duration of blade contact (~ 1 s) leads to $\leq 1/30$ the plastic sinkage associated with the typical wait times (30 s and 80 s). Figure 6, and its caption, helps to illustrate these points. Hence, following any of the normal load increments the ploughing depth due to ice crushing at the bow of the blade during a gliding test is ~ 0.051 mm,

Tests with loads up to 700 N were applied in the manner described above, where each incremental increase in load (100 N) was applied in about 2 seconds. Figure 6 shows the blade penetration vs time for the tests corresponding to normal loads in the range 300 – 700 N. The data for the 100 N and 200 N loads show a similar linear trend as in Figure 6, but have not been included because they were acquired on the previous day of testing, where the test sample surface location (vertically) was slightly different than the previous setup and this

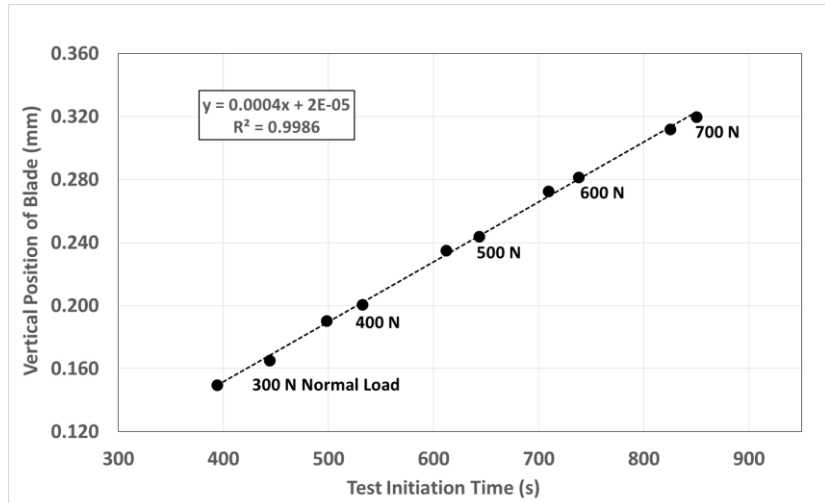


Figure 6. Vertical Position of the Blade vs Time at the start location for a series of gliding tests conducted in the same track. Solid-circle markers appear in pairs, where each pair corresponds to the first and second test at any given normal load. The magnitude of normal load, however, does not affect the rate of plastic sinkage, which is linear throughout the time span. Rather, the plastic sinkage is purely a function of the wait time interval between tests when some relatively arbitrary amount of normal loading is applied. A similar amount of ice is ploughed out of the track during the pair of tests after each load increment, that is, the track deepens throughout the series of gliding tests.

led to an offset in the data. The fit to the data in Figure 6 indicates a linear relationship of penetration with time, i.e. 0.0004 mm / s. Since the sectional profile of the bottom of the blade was precisely known (see Figure 7) one can calculate the amount of ice in profile that is removed for a given penetration.

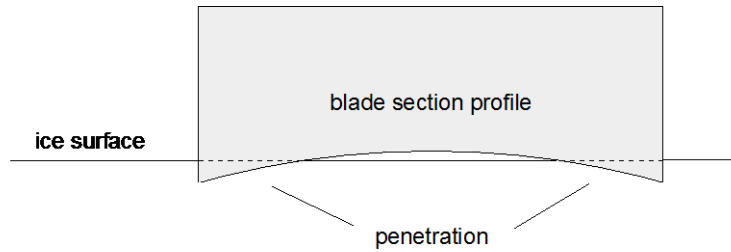


Figure 7. A sectional-view schematic showing the plastic penetration of the mock blade into the ice surface due to a normal load applied for a certain time. Note the 7 mm radius ‘hollow’ on the bottom of the blade.

For example, in principle if we consider the total penetration from the time associated with applying the 300 N normal load to the 700 N normal load, i.e. ~ 0.16 mm, we can determine that the sectional area for that penetration would be 0.1024 mm². For a glide distance of 1 mm this implies 0.1024 mm³ of ice would be removed. During the test program the normal loads were applied incrementally and the average wait time between the test before and the test after the load increments (as in Figure 6) was about ~ 72 s, corresponding to a plastic penetration of 0.0287 mm. This penetration for a 1 mm glide amounts to a volume of ice removed equal to 0.0287/0.16 x 0.1024 mm³ = 0.0184 mm³.

From Figure 8 the corresponding horizontal force for the mid-range normal load of 400 N is 5.4 N. Since we know from the video and post-test photographs of the glide track that all ice removed from the track during a glide test occurs due to crushing and the production and egress of the ice-particle/liquid slurry, it is reasonable to expect similar high-pressure values within the slurry that have been seen in various ice-crushing experiments. Pressure estimates from previous ice-crushing experiments,

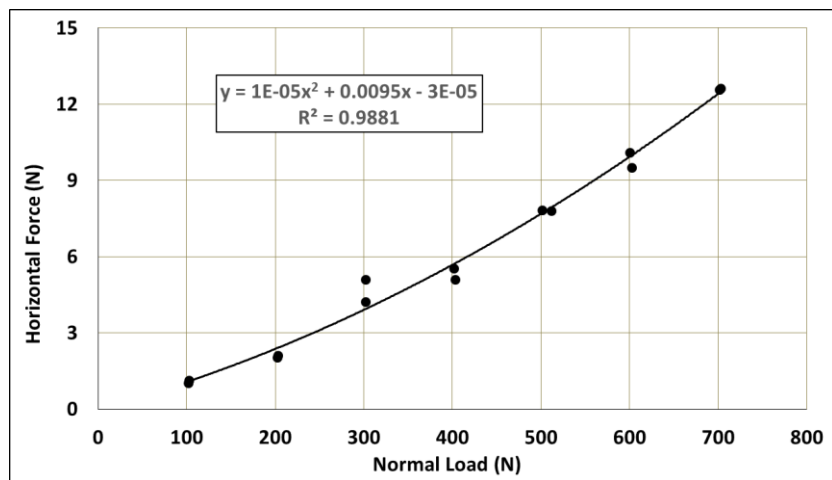


Figure 8. Horizontal Force vs Normal Load for gliding tests using the mock skate blade oriented in the glide direction. The gliding speed was 30 mm/s and the ambient test temperature was -5 °C. Note that the load associated with ploughing/spallation is roughly constant for each 100 N increment in load because the tests are run in the same track so that the amount of ice removed by ploughing is roughly the same for each test, whereas the friction force on the horizontal portion of the blade monotonically increases with the normal load.

some involving in situ observations of the slurry layer (e.g. Gagnon and Tulk, 2019), are in the range 20 – 70 MPa. So a slurry-layer pressure estimate of ~ 50 MPa would be reasonable. From the pressure and estimated volume of ice removed for 1 mm of glide the associated energy is $E = P \times V = 50 \text{ MPa} \times 0.0184 \text{ mm}^3 \approx 0.001 \text{ J}$. The volume of ice that this amount of energy can melt is 0.00329 mm^3 and the fractional amount of melt in the slurry is $0.00329 \text{ mm}^3 / 0.0184 \text{ mm}^3 \times 100 \approx 18 \%$ (by weight). The energy implies a ploughing force at the bow of the blade of ~ 1

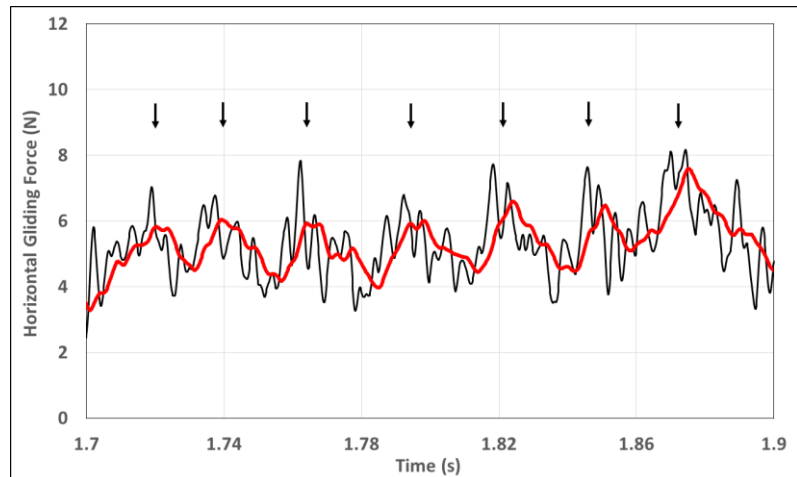


Figure 9. Horizontal gliding-force record associated with a test similar to that shown in Figures 1 and 2, where the normal load was 400 N. The spacing of the seven main peaks (indicated by arrows) may correspond to the time spacing of reasonably-anticipated spalling events at the bow of the blade, occurring at ~ 39 Hz. The other higher-frequency oscillations are due to the resonant frequency of the horizontal measurement/load equipment (roughly 200 Hz). The red trace corresponds to a running-average of the data that filters out the apparatus resonance.

N. The remaining 4.4 N of load can be attributed to the gliding friction of the rest of the blade with the ice along the track. A further note is that some segments of the horizontal load records from the gliding tests exhibit small regular oscillations that are suggestive of spallation events at the bow of the blade during gliding (Figure 9). Also note that corresponding small-amplitude (~ 1 N) oscillations were discernible in the normal load record. These observations are preliminary, however, and should be substantiated by further experiments, possibly utilizing high-speed imaging instrumentation and including careful post-test track analysis (as was done for the shaving tests discussed earlier).

The value of fractional melt of the slurry for the gliding tests is similar to (but somewhat higher) than those from the lateral shaving tests, and is also similar to values from other ice-crushing experiments (e.g. Gagnon and Tulk, 2019). The thin (< 0.1 mm thickness as estimated from edge-on views) wispy nature of the white material extruded from the sides of the frontal portion of the blade during gliding (Figures 10 and 11), that disintegrates into extremely fine powder when disturbed, is consistent with the presence of a thin mobile slurry layer during ice crushing, as has been observed before in various experiments (mentioned above). Our fractional melt estimate of the slurry (~ 18 %) for the gliding case is higher than that which was determined from the total volume of ice removed and the associated energy from the lateral-shaving tests (~ 12 %). However, there is no lack of consistency. More energy per unit volume of removed ice was consumed in the gliding case because all spallation debris at the bow was removed from the track by high-pressure compaction



Figure 10. Thin (< 0.1 mm) white sheet of wispy material sticking up from the ice surface along the sides of the glide track left after a number of tests. The material is the fully-frozen remnant of the thin slurry layer (originally 18 % liquid) that was squeezed out of the forward bow region of the blade during the test. The reader may expand the view on-screen to see fine details. Note that some slurry was also squeezed into the central area of the track where the hollow of the blade provided a small gap (as in Figure 7) between the ice surface and the blade.

imposed by the over-running blade. This caused further pulverization and inter-particle ice-on-ice crushing generating mobile slurry that augmented slurry produced on intact-ice hard-zone areas at the blade-ice interface. That is, all of the ice removed from the track was converted to slurry. In the lateral shaving case less material was converted to slurry because many unconfined pieces of the shattered spalls were not subjected to further pulverization/extrusion. This was evident from the post-test observation of the accumulated shaved material that showed spall debris (i.e. small chunks of intact ice) mixed with extruded slurry (see shaved material at the right of Figure 4).

Note that when the wispy material is swept away from the blade track after a test, one observes that the track is very smooth and has a consistent profile (Figures 11 and 12). There is no evidence of distorted grain boundaries from the original surface, or bulging of ice at the sides or in the center of the tracks, that would suggest actual plastic behaviour, as classically defined. Also, when squeezed from under a blade we might reasonably expect that a pure liquid layer would tend to pool and freeze as a solid ridge or mound, that is, have a look and form quite different from the observed wispy material that is essentially refrozen slurry that initially consists of roughly 18 % liquid.

To explain how ice is removed from the tracks in a manner that leaves the ice in the immediate proximity of the tracks virtually undisturbed, we turn to results and conclusions from other in situ observation studies of ice crushing in the brittle regime. The high-pressure zones in general have been shown to be regions where a thin squeeze-film slurry layer of pressurized melt and ice particles is present between the intact ice and the surface (similar to the blade/ice contact region in Figure 5). The viscous flow of this slurry layer generates heat



Figure 11. Bow portion of the blade track created by a number of glide tests. The two parallel, but separated, segments of the track (outlined) stem from the ‘hollow’ shown in the sectional profile of the blade (Figure 7). The ‘pointy’ regions on the ends of the segments are due to the upturn of the blade bow. The white material is the fully-frozen remnant of the slurry (~ 18 % liquid by weight) ejected at the bow during gliding. All ice that is removed from the track leaves in the form of slurry.



Figure 12. Glide track produced by a number of tests. The wispy fully-frozen slurry (as in Figures 10 and 11) has been swept away to reveal the smooth glide track that shows no signs of plastic deformation or mounds of refrozen melt at the sides or center.

that accounts for the rapid melting component of the removal of ice from the hard zones during ice crushing. A similar process occurs at ice-on-ice contact (Gagnon, 2013) of ice fragments in the surrounding crushed-ice matrix as it flows away from the high-pressure zones.

To further explain how ice particles can be created and entrained in the thin flowing slurry layer Gagnon and Tulk (2019) provided experimental evidence that tiny liquid Tyndall melt figures nucleate at the surface of the ice that is in contact with the

pressurized slurry layer and extend to a small depth in the ice during the rapid adiabatic increases in pressure that occur in ice during and between repetitive spalling events (Gagnon, 1999). The Tyndall figures could etch a fine texture of prominences on the ice surface that would break off, due to the shearing force of the flowing slurry, and become entrained in the flow. Note that the liquid fraction of the slurry is not created by pressure melting, which would involve the relatively slow process of heat conduction from the bulk ice and the crushing platen. Nor does pressure melting play a significant role in the continuous crushing of ice at rates in the brittle regime. Rather, the melt in the slurry layer is generated from heat created by the viscous flow of the pressurized slurry. That is, the flowing slurry generates heat that raises the ice surface temperature in immediate contact with it to the melting temperature and then causes melting. This happens extremely fast since the melting surface (the contacted hard-zone ice) and the heat generator (the flowing slurry) are in direct contact. The ice particles entrained in the slurry would also experience some melting.

To reiterate, the presence of tiny melt figures at the ice/blade interface during ice crushing might explain how ice particles can erode from the contacting ice surface due to the tenuous matrix of surface-weakening shallow-depth (< 0.1 mm) melt figures at the ice interface

during adiabatic pressure spikes. This could facilitate a unique erosive effect that occurs as the material in the top portion of this weakened layer is sheared off by, and entrained in, the ambient viscous flow of slurry.

CONCLUSIONS

The present tests and observations have shown that various characteristics of ice-crushing in the brittle regime (e.g. spallation and related load oscillations, and the slurry layer), as seen in larger-scale experiments, are also at play beneath ice-skating blades. While some previous theoretical studies have described a thin film of melt beneath gliding blades that is generated by friction (e.g. Le Berre and Pomeau, 2015; Lozowski et al., 2013; Van Leeuwen, 2017), our results are the first to report a thin slurry layer of ice particles and melt. The slurry layer was produced at the forward bow of the blade during gliding, and along the blade's edge during lateral shaving motions, where in both cases ice crushing was the progenitor. Since the slurry layer has been shown to be highly lubricating during ice crushing-friction tests (Gagnon, 2016), even on rough surfaces, we suggest that its role in ice skating is probably significant and worth further investigation.

ACKNOWLEDGEMENTS

The author thanks Austin Bugden for expert technical assistance during the experiments, and is grateful to NRC for accommodating this endeavor.

REFERENCES

- Gagnon, R.E., 1999. Consistent observations of ice crushing in laboratory tests and field experiments covering three orders of magnitude in scale. *Proceedings of POAC-99*. 2, pp. 858–869.
- Gagnon, R.E., 2013. High-speed imaging of ice-on-ice crushing. In: *Proceedings of POAC 2013*, Espoo, Finland.
- Gagnon, R.E., 2016. New friction mechanisms revealed by ice crushing-friction tests on high-roughness surfaces. *Cold Regions Science and Technology* 131 (2016) 1–9.
- Gagnon, R.E. and Tulk, C.A., 2019. Evidence for Tyndall melt-figure production during spallation-induced pressure spikes associated with ice crushing. *Cold Regions Science and Technology* 167 (2019) 102867.
- Le Berre, M. and Pomeau, Y., 2015. Theory of ice-skating. *International Journal of Non-Linear Mechanics* 75, DOI: 10.1016/j.ijnonlinmec.2015.02.004.
- Lozowski, E., Szilder, K., Maw, S., 2013. A model of ice friction for a speed skate blade. *Sports Engineering* 16 (4), 239–253.
- Van Leeuwen, J.M.J., 2017. Skating on Slippery Ice. *SciPost Phys.* 3, 042 (2017) DOI: 10.21468/SciPostPhys.3.6.042. arXiv:1706.08278v2 [cond-mat.other] 11 July, 2017.